https://doi.org/10.5194/essd-2024-338
Preprint. Discussion started: 9 September 2024

Open Access Earth System Science Data Discussions

A High Dense Temperature-Salinity Dataset Observed by Automatic Underwater Vehicles toward Mesoscale eddies' Evolutions and Associated Submesoscale Processes in South China Sea

Chunhua Qiu[1,2], Zhenyang Du[1,2], Jiancheng Yu[3], Huabin Mao[4], Haibo Tang[1,2], Zhenhui Yi[1,2], Jiawei Qiao[1,2], Dongxiao Wang[1,2,*] , Xiaoming Zhai[5], Yeqiang Shu[4]

1. School of Marine Sciences, Sun Yat-sen University, &Southern Marine Science and Engineering Guangdong Laboratory (Zhuhai), Guangzhou 510275, China

2. Guangdong Provincial Key Laboratory of Marine Resources and Coastal Engineering, School of Marine Sciences, Sun Yat-sen University, Guangzhou 510275, China

3. State Key Laboratory of Robotics, Shenyang Institute of Automation, Chinese Academy of Sciences, Shenyang 110016, China

4. State Key Laboratory of Tropical Oceanography, South China Sea Institute of Oceanology, Chinese Academy of Sciences, Guangzhou, China

5. Centre for Ocean and Atmospheric Sciences, School of Environmental Sciences, University of East Anglia, Norwich, UK

Corresponding author:

Dongxiao Wang

School of Marine Sciences,

Sun Yat-sen University

Email: dxwang@mail.sysu.edu.cn

https://doi.org/10.5194/essd-2024-338
Preprint. Discussion started: 9 September 2024

Open Access Earth System Science Data Discussions

Abstract. Marginal seas are usually fulfilled with strongly varying mesoscale eddies (MEs), which evolutions plays vital roles in regulating global oceanic energy equilibrium, triggering subemesoscale processes with strong vertical velocity, and inducing high biogeochemistry transport. But the temporal evolutions of MEs and submesoscale processes with several kilometers' resolutions are difficult to be measured by traditional observations with passive working mode. The automatic underwater gliders (AUGs) and vehicles (AUVs) positively observe oceanic motion, and could provide us spatiotemporal synchronization information for strongly varying MEs. Here, we present a 9-year high dense dataset of AUVs/AUGs observations in 2014-2022 in the South China Sea (SCS) can be downloaded from https://doi.org/10.57760/sciencedb.11996 (Qiu et al., 2024b). Totally, 9 AUG and 2 AUV cruise experiments were conducted, and 83 AUGs (2 AUVs) equipment were deployed with zonal and temporal resolutions of < 7 km and <6 hour. It covers the area of eddy's birth, propagation, and dissipation, presenting us the most complete data to investigate the evolution of MEs at different life stages. 40% of them reach resolutions < 1 km and < 1 hour, which provides us the dynamic characteristics of submesoscale instabilities across and along front at the eddy edge. This dataset has potential in improving the forecast accuracy in physical and biogeochemistry numerical model. Much more aggressive field investigation programs will be promoted by the NSFC in future.

Keywords: Automatic Underwater Vehicles; Mesoscale eddies; submesoscale processes; South China Sea

https://doi.org/10.5194/essd-2024-338
Preprint. Discussion started: 9 September 2024

1. Background

Marginal seas (such as, Gulf of Mexico, South China Sea, Mediterranean) are usually fulfilled with multi-scale oceanic motions, i.e. boundary current, mesoscale eddies (MEs; Rossby number $R_o = U/fL \approx 0.1$), and smaller scale processes ($R_o >$ 1). MEs, with spatial scale of 50–300 km and temporal scale of several weeks to months, play vital roles in the transport of matter and energy (Chelton et al., 2007; Morrow et al., 2004). They are numerous in the global ocean and also in the tropical marginal sea of South China Sea (SCS; Chen et al., 2011; Wang et al., 2003; Xiu et al., 2010). They easily generate by obtaining kinetic energy from large-scale current, and easily dissipate to submeso- or smaller- scale processes at the slope region via shear and baroclinic instabilities (Oey, 1995; Okkonen et al., 2003). Evolutions of MEs, with high geostrophic straining, favors the generation of submesoscale processes with several kilometers' spatial resolution (McWilliam, 2016), and requires high-accuracy, spatiotemporal synchronization and dense observations.

Observation plats include ship-cruise, satellite, Argo float, mooring, drifters, automatic unmanned vehicle (AUV), and automatic underwater gliders (AUG), etc. These plats have been utilized to detect variations of MEs in SCS (Table 1). Ship-cruise observations are the most traditional methods to investigate the MEs' general structures (Wang et al., 1987; Xu et al., 1996), but difficult to track their spatiotemporal evolutions. Satellite data provide wide surface information of MEs (i.e., temporal and spatial scales; Chelton et al., 2011) and air-sea interactions have been revealed (Ni et al., 2021; Small et al., 2008). Southwest of Taiwan Islands, northwest of Luzon Islands, Xisha Islands region, and east of Vietnam are the four main eddy birth pools (Hwang et al., 2000; Wang et al., 2003; Nan et al., 2011). After birth, MEs move westward, southwestward, or northwestward under the control of the first-baroclinic Rossby wave (Lin et al., 2007; Xiu et al., 2010; Chen et al., 2011). Since 2002, a large number of Argos have been deployed, providing routine measurements to describe vertical structures of MEs (He et al., 2018; Table 1). The spatiotemporal resolutions of Argo profiles are approximately 100 km and 10 days, which is difficult to capture the high-frequency variability of MEs

https://doi.org/10.5194/essd-2024-338
Preprint. Discussion started: 9 September 2024

and submesoscale processes (Table 1).

Table 1. Observation studies of ME in SCS. ME: mesoscale eddies

Ship Observation (CTD Station)	Dale, 1956	Cool pool near Vietnam
	Wang et al., 1987	Warm eddy near southwestern of Taiwan Islands
	Xu et al., 1996; Wang et al., 2001	Northwest of Luzon Islands, named Luzon cold eddy
	Li et al., 1998	A warm eddy in northeast of NSCS
	Chu et al., 1998	An eddy pair in central of SCS.
	Yang et al., 1998	Vietnam cold eddy
	Fang et al., 2002	Vietnam warm eddy
Satellite Observations (sea level anomaly; velocity)	Hwang et al., 2000; Wang et al., 2003; Nan et al., 2011a	Topex/Poseidon altimeter data, 94 cold eddy, 124 warm eddy. Southwest of Taiwan Islands, northwest of Luzon Islands, East of Vietnam.
	Lin et al., 2007; Chen et al., 2011; Xiu et al., 2010	Radius, life cycle, tracking, seasonal and interannual variations of mesoscale eddies
	He et al., 2016	The role of ENSO on interannual variation in Luzon Strait mesoscale eddies
	He et al., 2019	MEs' influence on Chl-a
Argo; Mooring	Li et al., 2022	Vertical tilt of Mesoscale eddy
	He et al., 2018	Reconstruction data combine altimeter and Argos, revisit the three-dimensional structures of ME
	Zhang et al., 2017	By using mooring array, investigate eddy looping from Luzon Strait

For this reason, our group has collected dense AUGs and AUVs observations across MEs. Attributed to the positively track, AUVs and AUGs become more and more important tools in exploring marine environment over last two decades. Many international products of AUGs were operated, such as "Seaglider", "Spray", "Slocum", "Deepglider", "SeaExplorer". Their product companies and related information are listed in Table 2. Multi-year AUGs have been successfully used in detecting strongly varying features in some marginal seas, such as estimation of trends of Gulf Stream (Todd and Ren, 2023), the water mass exchanges between Bay of Bengal and Arabian Sea (Rainville et al., 2022). We reported AUGs experiments since 2014 (Qiu et al., 2015), and made AUV experiments since 2018 (Huang et al., 2019; Qiu et al., 2020).

https://doi.org/10.5194/essd-2024-338
Preprint. Discussion started: 9 September 2024

Here, we present 9-year (2014-2022) AUVs and AUGs datasets in SCS, and try to show their potential abilities in detecting the evolutions of MEs and the associated submesoscale processes.

Table 2. Types of several popular underwater gliders

Types	Development Organizations
Seaglider	University of Washington
Spray	Scripps Institute of Oceanography and Woods Hole, https://spray.ucsd.edu/pub/rel/info/spray_description.php
Slocum serials	Webb Research Cor.
Deepglider / Oculus	Kongsberg Underwater Technology, Inc.
SeaExplorer glider	ACSA, Sep.5, 2013 https://www.marinetechnologynews.com/news/seaexplorer-underwater-glider-record-487228
Sea Wing	Shenyang Institute of Automation, Chinese Academy f Sciences https://baike.baidu.com/item/%E6%B0%B4%E4%B8%8B%E6%BB%91%E7%BF%94%E6%9C%BA/4560334
Petrel	Tianjin University; https://baike.baidu.com/item/%E2%80%9C%E6%B5%B7%E7%87%95%E2%80%9D%E5%8F%B7%E6%B0%B4%E4%B8%8B%E6%BB%91%E7%BF%94%E6%9C%BA/13977071

2. Data Description

2.1 AUG and AUV experiment sites

Different with Rainville et al (2022) and Todd and Ren (2023), most of our experiments aimed to detect the evolution of MEs or submesoscale processes. Two products of Chinese AUGs named “Sea Wing” and “Petrel” are utilized in revealing the development of MEs in this study. Since 2014, we have conducted 11 experiments, totally collecting 24498 temperature and salinity profiles, which is even more than those in Gulf Stream (Todd and Ren, 2023). 83 AUGs and 2 AUVs were deployed in northern SCS. The deploying time, installed sensors, and diving depths of AUGs/AUVs experiment were shown in Table 3. The gray highlighted the AUG network experiments, with number of AUGs $\geq$3. Such as, in the experiments of 2017, 2019 and 2020, more than 10 AUGs were deployed to detect the three-dimensional structures of the mesoscale eddies. The largest AUG network was conducted in 2021, including 50 AUGs, which was set to investigate eddy-current interaction.

https://doi.org/10.5194/essd-2024-338
Preprint. Discussion started: 9 September 2024

Table 3. Information of individual AUG/AUV experiment and the observing purpose. ME: Mesoscale Eddies

Number	Equipment	Time	Number of Qualified Profiles	Number of equipment	Sensor of equipment (*: with Shipped CTD; ##: with DO and Chl-a sensors; ++: Velocity)	Diving depth of equipment	Observing Purpose
1	AUG	Sept. 19- Oct. 15, 2014; 26 days	227	1 AUG	Seabird Glider Payload CTD(GPCTD)	1000 m	Mixed layer heat budget; sea trials
2	AUG	Apr. 18-Jul. 6, 2015; 78 days	446	3 AUGs Network	Seabird Glider Payload CTD(GPCTD)	1000 m	Structures of ME
3	AUG	Jul. 14-Aug. 13, 2017 30 days	3016	10 AUGs, Network	Seabird Glider Payload CTD(GPCTD); Aanderaa oxygen optode probes and WETLabs fluorescent probes ##	300 m (3) 1000 m (7)	ME response to TC
4	AUG	Apr. 22-May 23, 2018; 31 days	239	1 AUG, Virtual mooring	Seabird Glider Payload CTD(GPCTD)	1000 m	Structures of ME
5	AUG	Jul. 13- Sept. 30, 2019; 77 days	15840	50 AUGs, Network	Seabird Glider Payload CTD(GPCTD) *	300 m (4) 1000 m (42) 4500 m (4)	Slope intrusion of ME
6	AUV	Sept. 18- Oct. 23, 2019; 35 days	143	1 AUV	SBE37 CTD; DVL++	300 m	Evolution of ME
7	AUG	Jun. 26- Aug. 27, 2020; 60 days	3515	12 AUGs	Seabird Glider Payload CTD(GPCTD)	1000 m	Slope current
8	AUG	Jul. 26- Aug. 8, 2021; 13 days	467	2 AUGs	RBR legato CTD	300 m (1) 1000 m (1)	Edge of ME
9	AUG	Aug. 7- Aug. 27, 2021; 20 days	219	2 AUGs	Seabird Glider Payload CTD(GPCTD)	1000 m	Edge of ME
10	AUV	May 9- Jul. 29, 2021; 80 days	169	1 AUV	SBE37 CTD	300 m	Evolution of ME
11	AUG	Jun. 23- Jul. 6, 2022; 13 days	217	2 AUGs	Seabird Glider Payload CTD(GPCTD)	1000 m	Edge of ME
Total	/	463 days	24498	83 AUGs, 2 AUVs	/	/	Structures and evolution of ME

https://doi.org/10.5194/essd-2024-338
Preprint. Discussion started: 9 September 2024

Earth System Science Data
Open Access
Discussions

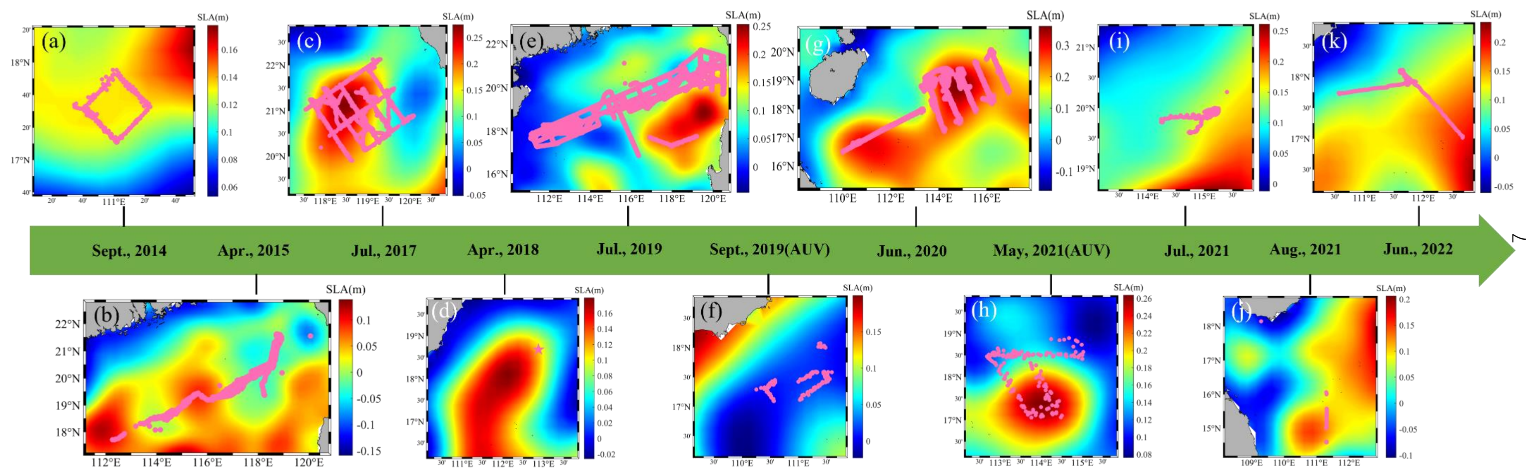

Figure 1. Time line of AUG and AUV observation mapping, with sea level anomaly (SLA, shading colors) and observation casts (pink points). (a) September, 2014; (b) April, 2015; (c) July, 2017; (d) April, 2018; (e) July, 2019; (f) September, 2019; (g) June, 2020; (h) May, 2021; (i) July, 2021; (j) August, 2021; and (k) June, 2022.

https://doi.org/10.5194/essd-2024-338
Preprint. Discussion started: 9 September 2024

2.2 Intercomparison of AUGs / AUVs resolution

The AUGs and AUVs positions with the mean sea level anomalies (SLAs) during experiment time were shown in Figure 1. Note that all the AUGs and AUVs crossed MEs with positive/negative SLAs. The spatial and temporal resolutions of samples were presented in Figure 2. The dominant spatial resolution (blue bars) was 4-7 km in 2014, 2015, and 2019, while it was less than 3 km in other years. In 2017 (Figure 2c), July 2021 (Figure 2f) and 2022 (Figure 2h), the temporal resolution of AUGs achieved 1-2 hours, while it was 4-7 hours in other experiments. It indicates that all of the experiments could resolve the MEs (spatial scale of 50-300 km), and 40% of them could be used to resolve submesoscale processes (spatial scale of <3 km).

https://doi.org/10.5194/essd-2024-338
Preprint. Discussion started: 9 September 2024

Open Access Earth System Science Data Discussions

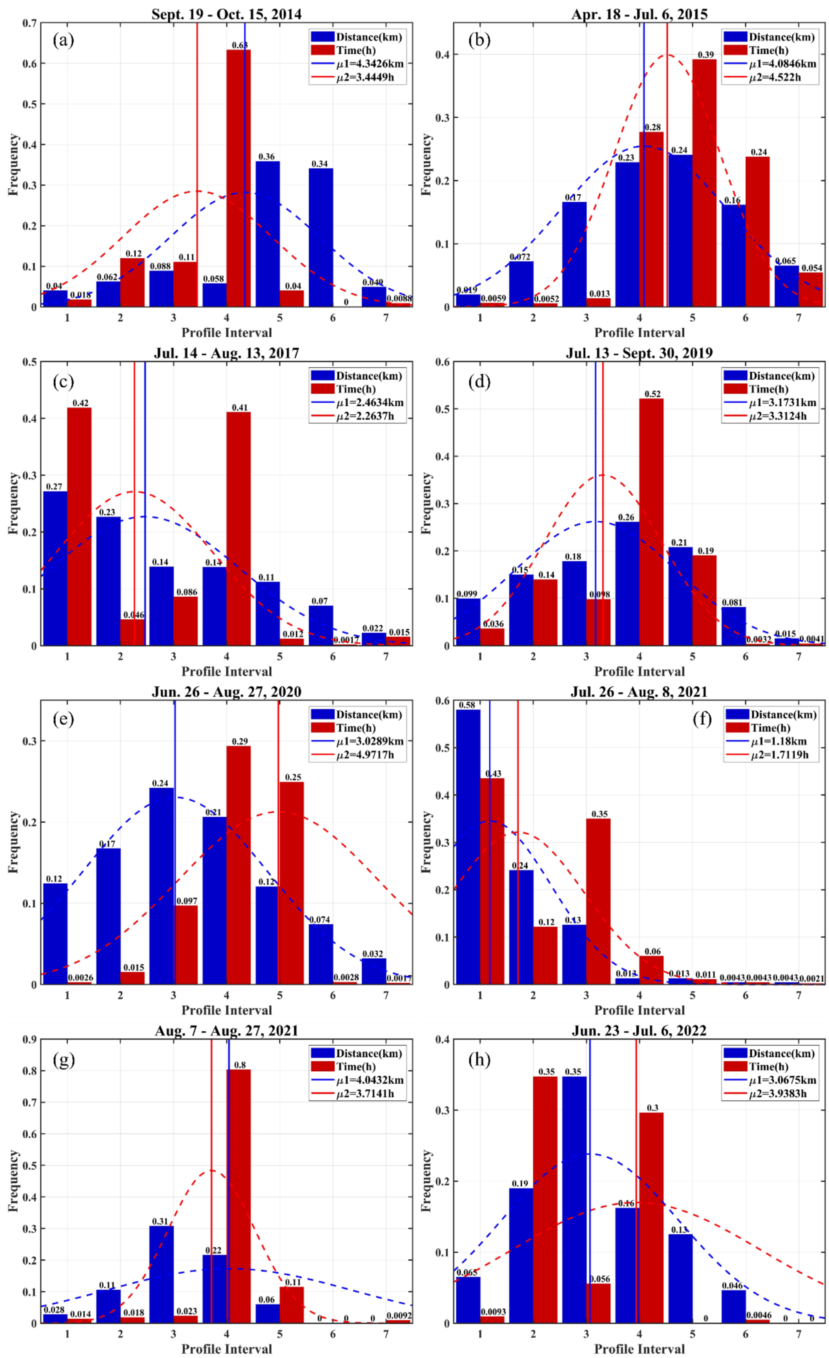

Figure 2. Frequency of spatial (blue bar) and temporal (red bar) sample interval. The red and blue bars (dashed red and blue lines) denote probabilities of spatial and time interval (the normal distributions of spatial and time intervals), respectively.

https://doi.org/10.5194/essd-2024-338
Preprint. Discussion started: 9 September 2024

Open Access Earth System Science Data Discussions

3 Data Quality Control Method

Before investigating the three-dimensional structures of MEs, we did quality control for the AUGs and AUVs.

3.1 Quality control for AUG data

Two products of Chinese AUGs named "Sea-wing" and "Petrel" were used in this study. The communication and navigation subsystem contain iridium satellite communication devices, wireless communication devices, a precision navigation attitude sensor, a Global Positioning System (GPS) device, a pressure meter, and obstacle avoidance sonar. A conductivity-temperature-depth (CTD) sensor with ~6 s sampling resolutions has been installed on the two AUG products.

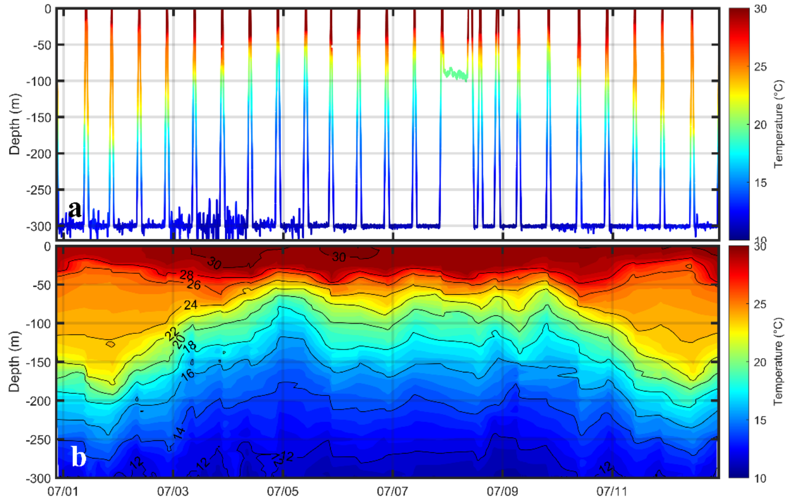

Figure 3. Illustration of (a) original, and (b) interpolated data after quality control. The AUV duration is in July 2021.

Before investigating oceanic phenomena, we did data quality control as follows: (1) sorted the vertical depth values and removed any duplicate depth values; (2) excluded the data with temperature/salinity larger than 35 °C/35 psu; (3) interpolated all the temperature/salinity profiles into 1-m interval vertically; (4) calibrated the salinity data by removing the thermal lag effect following Morison et al (1994); (5) calculated temperature difference between each profile and mean profile from World Ocean Atlas (WOA) data, and then excluded the difference larger than 3 °C. This method was

https://doi.org/10.5194/essd-2024-338
Preprint. Discussion started: 9 September 2024

adopted in Qiu et al (2015;2019), Chu and Fan (2010), and Yi et al (2022).

We have validated the AUG observed temperature and salinity profiles with ship observed data during July, 2019 (black star in Figure 1e; Figure 4). The mean bias of temperature is 0.05 °C, and that of salinity is 0.01 psu. The vertical temperature/salinity profiles of ship and AUG installed CTD are consistent, supporting that the data are credible.

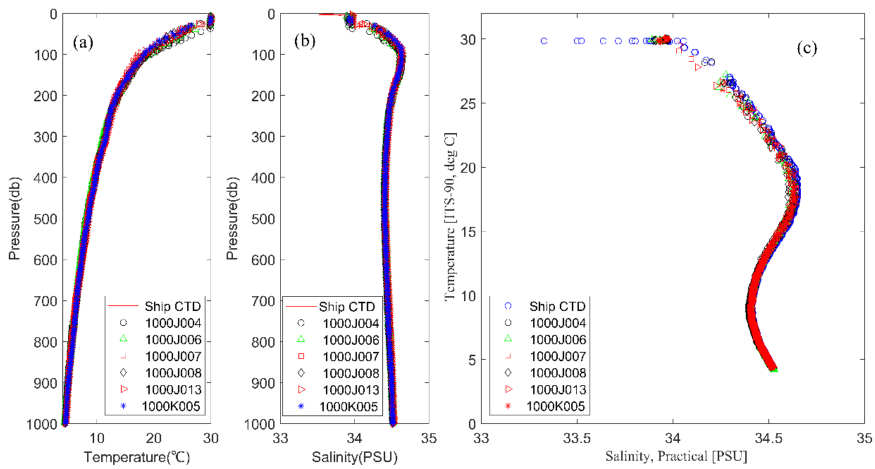

Figure 4. Comparison of (a) temperature, (b)salinity, and (c) temperature-salinity scatter plots between ship installed CTD and AUV installed CTD at station (112.0661°E, 17.7778°N). Red line in (a) and (b) is the ship measured values. Different symbols are the different AUG.

3.2 Quality control for AUV data

Both CTD and GPS instrument were installed on the "Sea-Whale 2000" AUV. This AUV was designed by Institute of Shenyang Automation, Chinese Academy of Sciences. It could operate in two modes, a "sawtooth-like" mode and a "cruise" mode at a depth of 300 m (Huang et al., 2019).

In the "sawtooth-like" mode, the data quality control procedures are the same as those for AUGs. Figures 3 and 4 show the AUV observed temperature after data-quality. In "cruise" mode, the AUV navigates at the depth of around 300 m. Following Qiu et al (2020), we firstly transformed the temperature and salinity at depth z to those at 300 m using a linear regression method ($T' = 0.008z' + 0.017; S' = -0.0002z' + 0.0006$),

https://doi.org/10.5194/essd-2024-338
Preprint. Discussion started: 9 September 2024

$$T' = T_z - T_{mean}, \quad (1a)$$

$$S' = S_z - S_{mean}, \quad (1b)$$

where T_{mean} is averaged using a 10-point smooth average, which could maintain the spatial variations from 20 to 30 km. Depth anomaly is defined as the measured depth minus 300 m, $z' = z - 300$, and the temperature and salinity anomalies as $T'$and S', respectively. We compared this method with the potential temperature algorithm, and the temperatures obtained at 300 m were highly consistent.

4. Data Application

4.1 Intra-thermocline (Subsurface) MEs observed by AUGs and AUVs

Cross-eddy tracks of AUG or AUV could observe both the warm core and cold cores (Figure 4). In April 2015, one AUG crossed a warm eddy, and observed a subsurface warm core (Figure 1b & Figure 5a). The warm core ranges from 50-500 m depth with radius about 100 km, which is termed as intra-thermocline anticyclone and has been reported in Shu et al (2016). Qiu et al (2019) utilized the same experimental dataset to investigate the asymmetry structures of this intra-thermocline eddies, suggesting that the centrifugal force should be taken into account when revealing the velocity of MEs, i.e. gradient wind theory. This gradient wind theory has been cited in a deriving global cyclogeostrophic currents data (Cao et al. 2023). In June 2020 (Figures 1g & 5d-f), one AUG captured a subsurface cold eddy with a negative temperature and positive salinity core. And the highly dense core ranged from surface to 500 m depth. Above all, single AUG/AUV could capture both the surface and the intra-thermocline eddy's position, range and strength.

https://doi.org/10.5194/essd-2024-338
Preprint. Discussion started: 9 September 2024

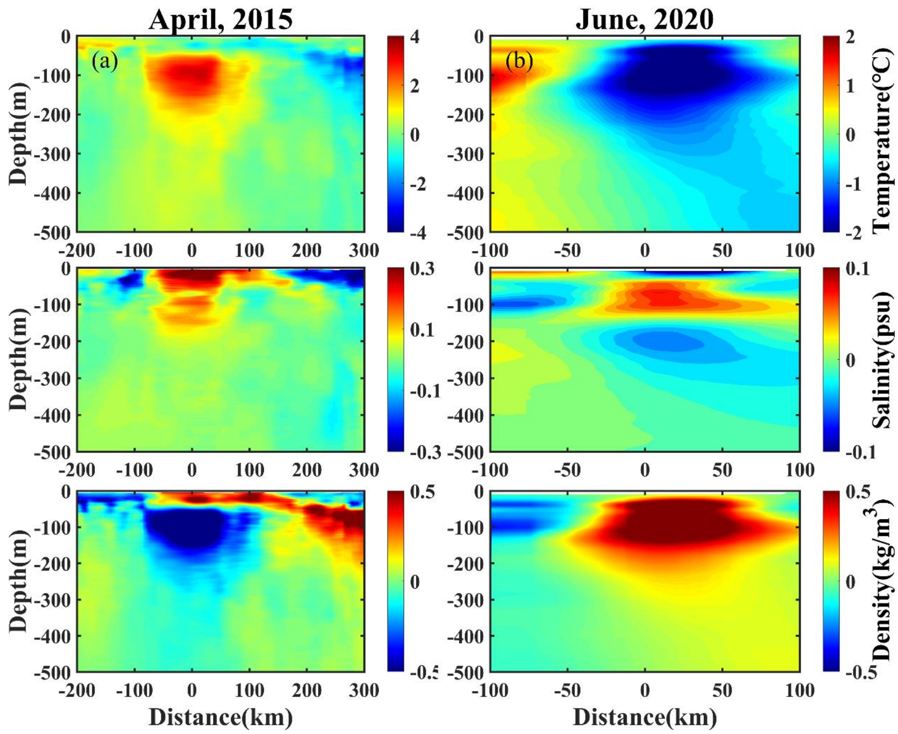

Figure 5. Projected depth plot of temperature anomaly (upper panels), salinity anomaly (middle panels), and density anomaly (lower panels) in (a)April, 2015 and (b)June, 2020.

AUG/AUV could track the development of intra-thermocline MEs. During developing stage, MEs can easily deform and may cause cross-slope transports at the continental slope (Wang et al., 2018; Su et al., 2020; Qiu et al., 2022), and produce submesoscale process (Dong et al., 2018; Yang et al., 2019). To observe the development of ME, "Sea-Whale 2000" AUV have traversed an anticyclonic ME using 5 repeated rectangular tracks from May to July 2021(Figure 1h). This experiment was supported by National Key R&D Program.

An anti-cyclonic eddy with low Brunt-Väisälä frequency squared value ($N^2 = \frac{1}{\rho}\frac{d\rho}{dz} < 10^{-4}$ s^{-1}), located in the subsurface layer from 50-200 m depth, and existed as an intra-thermocline anticyclonic eddy (Figure 6). The repeated cruise of AUV was separated to five stages, termed as T1(June 8-11), T2 (June 19-23), T3 (June 29- July

https://doi.org/10.5194/essd-2024-338
Preprint. Discussion started: 9 September 2024

4), T4 (July 10- 15), and T5 (July 21-26). Taking 22.5 kg/m^3 and 23.5 kg/m^3 as the upper and lower boundary of the intra-thermocline ME, we calculated the area and the mean temperature within the mesoscale eddy. The area and mean temperature decreased from T1-T3, and then increased from T4-T5, indicating the intra-thermocline anticyclonic eddy weakened from T1-T3 and strengthened from T4-T5. This development has been described in detail by Qiao et al (2023), who found the eddy moved eastward during T1-T3 and got stuck during T4-T5.

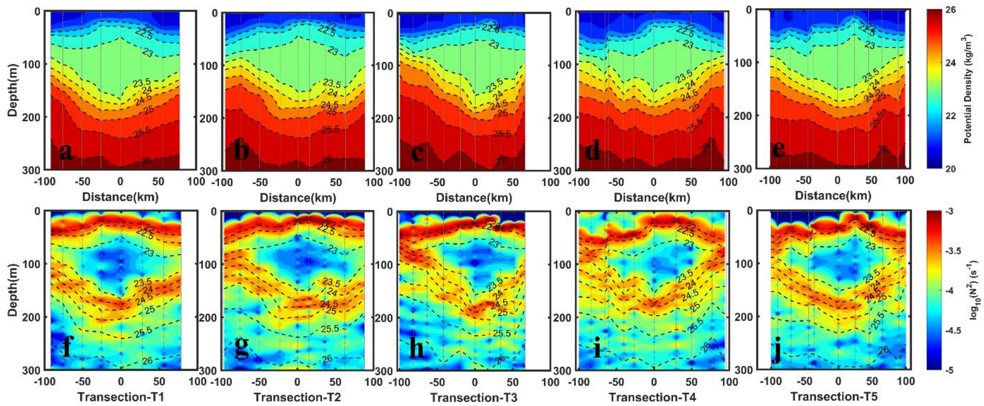

Figure 6. The profiles of density (upper panel) and Brunt frequency (lower panel) during (a,f)T1, (b,g)T2, (c,h)T3, (d, i)T4, (e, j)T5 period, which was 06/08-06/11,06/19-06/23,06/29-07/04,07/10-07/15,07/21-07/26, respectively.

4.2 Vertical Tilt of MEs at different life-stages observed by AUGs

Several systematic AUG networks were conducted in 2015, 2017, 2019, and 2020. A whole life cycle of ME usually experiences birth, developing, mature and dissipate stages (Zhang and Qiu, 2018; Yang et al., 2019), and the eddy's age has suggested to influence on the kinetic energy of ME. Luzon strait is an eddy birth zone, where Kuroshio branch intrudes the SCS (Chen et al., 2011; Su et al., 2020). And then, most of the eddies move westward to the continental shelf zone under the modulation of Rossby wave, finally dissipate in Dongsha Islands, Xisha Islands or merged with other eddies (Yang et al., 2019; Su et al., 2020; Qiu et al., 2022).

The systematic AUG experiments provide us probability in capturing the different

https://doi.org/10.5194/essd-2024-338
Preprint. Discussion started: 9 September 2024

vertical structures of MEs at different life stages. After data quality, we firstly mapped the temperature and salinity data onto 1 km × 1 km × 1 m grid, and then calculated the water density, ρ. Finally, we derived the geostrophic velocity, v_g, by using thermal-wind relationships,

$$v_g(x,y,z) = v_0 - \frac{g}{f\rho_0}\int_{z0}^{z}\left(\frac{\partial\rho(x,y,z)}{\partial x} + \frac{\partial\rho(x,y,z)}{\partial y}\right)dz, \qquad (3)$$

where ρ_0 is the referenced water density, f is the Coriolis frequency, v_0 is the referenced geostrophic velocity at depth 1000 m and assumed to be 0.

Figure 7a-b depicts the three-dimensional temperature and velocity structures of a ME (120 °E) at birth stage, as observed by 12 AUGs in July 2019 (Figure 1e&6a-b). A warm core was located at subsurface layer and the eddy center exhibited a northeastward vertical tilt (solid black line). In July 2017 (Figures 1c & 6c-d), 10 AUGs were deployed westward to the Luzon Strait (119 °E). This eddy was in its developing phase and possessed a significant eastward vertical tilt from deep up to surface, reaching depths deeper than 500 m. The eastward vertical tilt is suggested to have been induced by the background current, westward propagation of Rossby Waves (e.g., Qiu et al., 2015; Zhang et al., 2016; Li et al., 2019), and advection background temperature gradient (e.g., Bonnici& Billant, 2020; Gaube et al., 2015; Li, Wang, et al., 2020). Throughout this experiment, the AUGs encountered the tropical storm "Haitang", results in that the ME underwent horizontal deformation, giving rise to submesoscale processes (Yi et al., 2022; Yi et al., 2024).

In June 2020, 6 AUGs were deployed across another warm ME in the shelf region (Figures 1g and 6e-h). The eddy was under dissipating stage due to the steep topography, displaying a significant southwestward tilt from a depth of 500 m to surface (Figure 7e-7f). This kind of southwestward vertical tilt was revealed by potential vorticity in a numerical model (Qiu et al., 2022), which was attributed to shallower water depth to the west of mesoscale eddies, and caused asymmetries of the velocities within the MEs. Qiao et al (2023) also captured an eastward movement of a ME by using AUV observations in June 2021(Figure 1h). Based on tensor decomposition of barotropic instability energy, they suggested wave-current interaction played the most important

https://doi.org/10.5194/essd-2024-338
Preprint. Discussion started: 9 September 2024

Open Access
Earth System Science Data
Discussions

role in the development and propagation of this eddy.

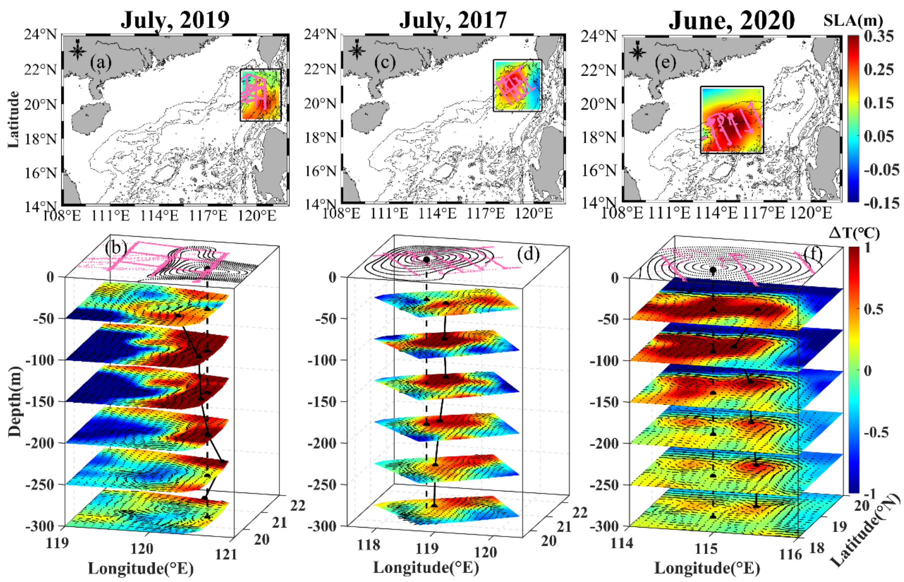

Figure 7. Eddy structures during periods of (a-b) eddy burst, (c-d) westward movement, and (e-f) dissipation along slope movements. SLA and AUGs' positions are superimposed in upper panels (a, c, e), isobaths are represented by solid lines. The AUG observed temperature and derived geostrophic velocities are in the 3D plots (b, d, f). Pink lines are the tracks of AUGs. Dashed lines denote the centers of mesoscale eddies from SLA fields, and solid dot lines are the centers from warm cores.

4.3 Submesoscale instabilities at the edge of MEs observed by AUGs

Fine structures, i.e., submesoscale process, usually occurs within MEs, either at the eddy edge (front; filament) or entrained in the eddy center, in terms of spiral structures or "eye-cat" structures (Zhang and Qiu, 2018; Ni et al., 2021; Hu et al., 2023; Qiu et al., 2024). They could cascade kinetic energy downward to turbulent scale via symmetric or centrifugal instabilities, and also induce kinetic energy inverse cascade to MEs via mixed layer baroclinic instabilities (i.e., Fox-Kemper et al., 2008; McWilliams, 2016). However, the submesoscale processes within MEs are difficult to be observed by Argo with 10-day's temporal resolution. Tang et al. (2022) attempted to observe submesoscale fronts using NAVIS float, and found that mixed-layer baroclinic instability dominated this frontogenesis. Qiu et al. (2019) and Shang et al (2023) have

https://doi.org/10.5194/essd-2024-338
Preprint. Discussion started: 9 September 2024

captured the submesoscale front at the eddy's edge by using a "virtual mooring" AUG observation. As passively driven by flow, NAVIS can only observe submesoscale process in an approximate Lagrangian fashion, whereas AUGs traversing a front could provide us both the cross-front and along-front information, depending on our observational scheme.

In our datasets, 40% of AUG observations have high spatiotemporal resolutions (<3 km, <4 h; Figure 2), which are fine enough to capture the submesoscale processes positively. Here, we present two examples of submesoscale instabilities at the edge of MEs to show the advantages of AUG observations.

As shown in Figure 8a, 4 diving AUGs were deployed at the eddy's edge (front) in 2017. 3 AUGs cross the front and 1 AUG tracks along the front. All of them successfully observed the submesoscale instabilities. Following Thomas *et al* (2013), the converted angle of the Richardson number, ϕ_{Ri}, can also be used to determine the nature of the instability:

$$\phi_{Ri} = tan^{-1}\left(-\frac{1}{Ri}\right) = tan^{-1}\left(\frac{|\nabla\cdot b|^2}{N^2\cdot f^2}\right), \quad (3a)$$

$$Ri \approx Ri_g = \frac{N^2}{\left(\frac{\partial v_g}{\partial z}\right)^2} = \frac{N^2\cdot f^2}{|\nabla\cdot b|^2} < \frac{f}{\zeta_g}, \text{ and } f\cdot\zeta_g > 0. \quad (3b)$$

where f is the Coriolis parameter, and $\vec{v}_g$ is the geostrophic velocity. $b = -g\rho/\rho_0$, is the buoyancy flux, g is the gravitational acceleration, and ρ is the seawater density, and ρ_0 is the reference density. $N^2 = \partial b/\partial z$ is the vertical buoyancy frequency. $\zeta_g = curl(\overrightarrow{v_g})$ is the vertical relative vorticity. ϕ_{Ri} can be used to judge when instability occurs. For anticyclonic eddies, inertial instability or symmetric instability occurs when $-45° < \phi_{Ri} < \phi_c$; symmetric instability occurs when $-90° < \phi_{Ri} < -45°$; symmetry instability or gravitational instability occurs when $-135° < \phi_{Ri} < -90°$; and gravitational instability occurs when $-180° < \phi_{Ri} < -135°$.

Figure 8a shows that AUGs observed several types of submesoscale instabilities, in terms of gravity instability, symmetric instability and mixed instabilities from symmetric and centrifugal instabilities at the anticyclonic eddy's edge. Figure 8b shows submesoscale instabilities in 2019. In this case, gravity instability dominates the upper

https://doi.org/10.5194/essd-2024-338
Preprint. Discussion started: 9 September 2024

Open Access Earth System Science Data Discussions

mixed layer. Symmetric and centrifugal instabilities are not significant. These two cases provide us enough information to detect frontal genesis processes in Euler filed, while Navis or Argos provide frontal information in Lagrange view.

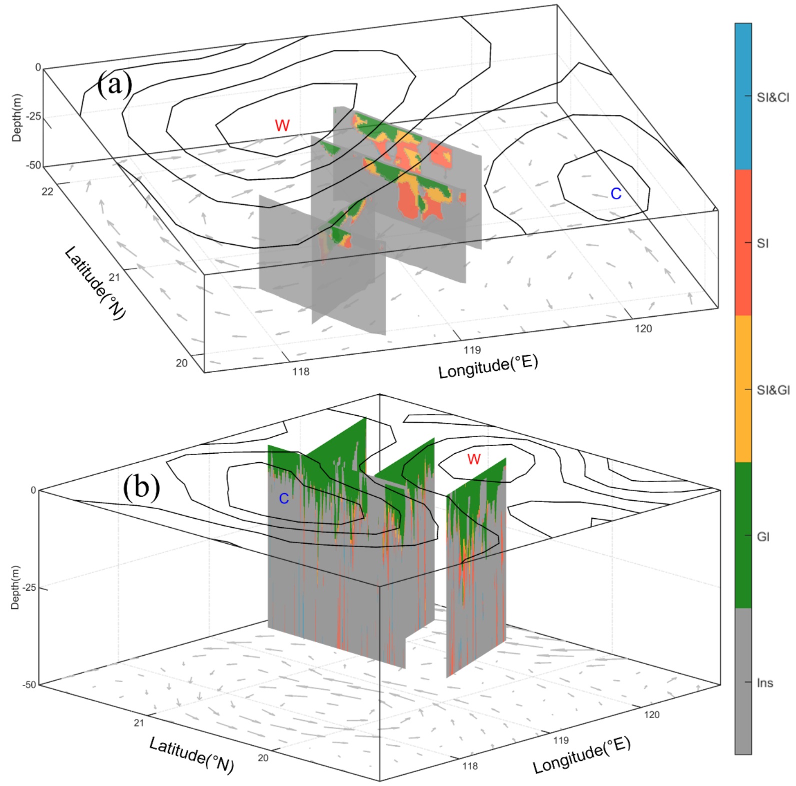

Figure 8. Analyzed submesoscale instabilities at the edge of mesoscale eddies. (a)in 2017, and (b) in 2019. SI: symmetric instability; CI: centrifugal instability; GI: gravity instability. W: anticyclonic eddy; C: cyclonic eddy. Isolines are the sea level anomaly.

5. Data availability

The dataset of AUV and AUG used in this manuscript was deposited in Science Data Bank, whose DOI is https://doi.org/10.57760/sciencedb.11996 (Qiu et al., 2024b).

6. Conclusions and Potential Future Plan

https://doi.org/10.5194/essd-2024-338
Preprint. Discussion started: 9 September 2024

Open Access Earth System Science Data Discussions

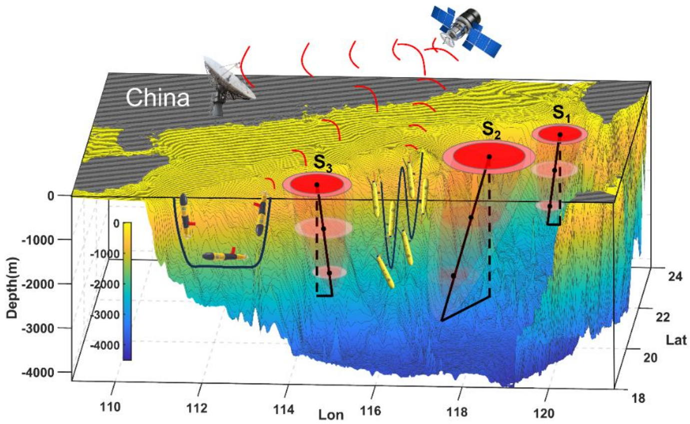

Figure 9. Scheme of AUGs observed mesoscale eddies at different life stages in the northern SCS. S1: birth stage; S2: developing/mature stage; S3: dissipating stage.

Based on 9-year AUVs and AUGs observations in SCS, we obtained high-resolution temperature and salinity profiles datasets in SCS. The dataset provides 24498 profiles and covers 463 days' experiments, including 11 experiments from 83 AUGs and 2 AUVs. To our knowledge, the 9-year dataset is enough in detecting the horizontal asymmetry, vertical tilt, temporal evolution, life cycle of MEs (Figure 9), and the associated submesoscale processes. The dataset supports us to investigate the subsurface MEs, revealing eddy-current and eddy-topography interactions successfully. However, to understand the feedback of MEs to the variability of larger scale current, i.e. western boundary current, routine AUGs and AUVs observations are needed in future.

Besides tracking MEs, AUGs and AUVs have been proved to positively capture more smaller scale oceanic process, such as internal tide (Gao et al., 2024), turbulences by using turbulent parameterization schemes (Qi et al, 2020). And AUGs/AUV installed with more sensors could also provide us geochemical parameters (e.g., Yi et al., 2022), presenting the potential ability in improving the forecast accuracy in physical and biogeochemical numerical model. More projects gathering AUVs network are ongoing and will be promoted in future.

https://doi.org/10.5194/essd-2024-338
Preprint. Discussion started: 9 September 2024

Author contributions

Conceptualization: DX, JC; data curation: CH, ZY, HB, ZH, HB, JW, YQ; formal analysis: CH, ZY; funding acquisition: CH, DX, JC; investigation: CH, DX, JC; methodology: CH, DX, JC; project administration: CH, DX, JC; software: CH, DX; supervision: CH, DX; validation: XM, DX; writing: CH, XM. All the authors have read and agreed to the published version of the manuscript.

Financial support

This study was supported by the National Natural Science Foundation of China (Grant No. 42376011; 41976002), National Key R&D Plan Program (No.2017YFC0305804).

Competing interests

The contact author has declared that none of the authors has any competing interests.

Acknowledgements

We acknowledge all the colleagues and project members who have contributed to the design of AUGs and AUVs, the sea experiments and data processing in the past. Many scientists and engineers have participated in active surveys and mappings. Their work provided basic high-quality materials.

Disclaimer

Publisher's note: Copernicus Publications remains neutral with regard to jurisdictional claims made in the text, published maps, institutional affiliations, or any other geographical representation in this paper. While Copernicus Publications makes every effort to include appropriate place names, the final responsibility lies with the authors.

https://doi.org/10.5194/essd-2024-338
Preprint. Discussion started: 9 September 2024

References:

Cao, Y., Dong, C., Stegner, A., Bethel, B. J., Li, C., Dong, J., et al. (2023). Global sea surface cyclogeostrophic currents derived from satellite altimetry data. *Journal of Geophysical Research: Oceans*, 128, e2022JC019357. https://doi.org/10.1029/2022JC01935

Chen, G., Hou, Y., Chu, X. Mesoscale eddies in the South China Sea: Mean properties, spatiotemporal variability, and impact on thermohaline structure. *Journal of Geophysical Research-Oceans*, 2011, 116, C06018. https://doi.org/10.1029/2010JC006716

Chelton, D., Schlax, M., Samelson, R., de Szoeke, R. Global observations of large oceanic eddies. *Geophysical Research Letters*, 2007, *34*(15), L15606. https://doi.org/10.1029/2007GL030812

Chelton, D., Schlax, M., Samelson, R. Global observations of nonlinear mesoscale eddies. *Progress in Oceanography*, 2011, 91 (2): 167–216, doi:10.1016/j.pocean.2011.01.002.

Chu, P., Chen, Y., Lu, S. Wind-driven South China Sea deep basin warm-core/cool-core eddies. *Journal of Oceanography*, 1998, 54(4), 347-360. doi: 10.1007/bf02742619.

Chu, P., Fan, C. Optimal linear fitting for objective determination of ocean mixed layer depth from glider profiles. *Journal of Atmospheric and Oceanic Technology*, 2010, 27, 1893–1898.

Dale, W. Winds and drift currents in the South China Sea. *Malayan Journal of Tropical Geography*, 1956, 8, 1-31.

Dong, C., Mcwilliams, J., C., Liu, Y., Chen D. Global heat and salt transports by eddy movement. *Nature Communications*, 2014, 5(2), 3294.

Dong, J., Zhong, Y. The spatiotemporal features of submesoscale processes in the northeastern South China Sea. *Acta Oceanology Sinica*, 2018, 37(11), 8-18. https://doi.org/10.1007/s13131-018-1277-2

Fang, W., Fang, G., Shi, P., Huang, Q., Xie, Q. Seasonal structures of upper layer circulation in the southern South China Sea from in situ observations. *Journal of Geophysical Research: Oceans*, 2002, 107(C11), 23-1-23-2. doi: 10.1029/2002JC001343.

Fox-Kemper, B., Ferrari, R., Hallberg, R. Parameterization of mixed layer eddies. Part I: Theory and diagnosis. *Journal of Physical Oceanography*, 2008, 38(6), 1145-1165. https://doi.org/10.1175/2007JPO3792.1

Gao, Z., Chen, Z., Huang, X., Yang, H., Wang, Y., Ma, W., & Luo, C. (2024). Estimating the energy flux of internal tides in the northern South China Sea using underwater gliders. *Journal of Geophysical Research: Oceans*, 129, e2023JC020385. https://doi.org/10.1029/ 2023JC020385

He, Q., Zhan, H., Cai, S., He, Y., Huang, G., Zhan, W. A new assessment of mesoscale eddies in the South China Sea: surface features, three-dimensional structures, and thermohaline transports. *Journal of Geophysical Research: Oceans*, 2018, 123(7), 4906-4929. https://doi.org/10.1029/2018JC014054

He, Q., Zhan, H., Xu, J., Cai, S., Zhan, W., Zhou, L., Zha, G. Eddy-induced chlorophyll anomalies inthe western South China Sea. *Journal of Geophysical Research: Oceans*, 2019, 124, https://doi.org/10.1029/2019JC015371.

He, Y., Xie, J., Cai, S. Interannual variability of winter eddy patterns in the eastern South China Sea. *Geophysical Research Letters*, 2016, 43(10), 5185-5193. doi: 10.1002/2016GL068842.

Hu, Z., Lin, H., Liu Z., Cao Z., Zhang F., Jiang Z., Zhang Y., Zhou K., and Dai M. Observations of a filamentous intrusion and vigorous submesoscale turbulence within a cyclonic mesoscale eddy, *Journal of Physical Oceanography*, 2023, 53(6), 1615–1627.

Huang, Y., Qiao, J., Yu, J., Wang, Z., Xie, Z., Liu, K. Sea-Whale 2000: a long-range hybrid

https://doi.org/10.5194/essd-2024-338
Preprint. Discussion started: 9 September 2024

autonomous underwater vehicle for ocean observations. *OCEANS 2019 - Marseille*, Marseille, France, 2019, 1-6, doi: 10.1109/OCEANSE.2019.8867050.

Hwang, C., Chen, S. Circulations and eddies over the South China Sea derived from TOPEX/Poseidon altimetry. *Journal of Geophysical Research: Oceans*, 2000, 105(C10), 23943-23965. doi: 10.1029/2000JC900092.

Li, H., Xu, F., Wang, G. Global mapping of mesoscale eddy vertical tilt. *Journal of Geophysical Research: Oceans*, 2022, 127, e2022JC019131. https://doi.org/10.1029/2022JC019131

Li, L., Worth. D., Nowlin, J., Su. J. Anticyclonic rings from the Kuroshio in the South China Sea. *Deep Sea Research Part I*, 1998, 45, 1469-1482. doi: 10.1016/s0967-0637(98)00026-0.

Lin, X., Dong, C., Chen, D., Liu, Y., Yang, J., Zou, B., Guan, Y. Three-dimensional properties of mesoscale eddies in the South China Sea based on eddy-resolving model output. *Deep-Sea Research Part I: Oceanographic Research Papers*, 2015, 99, 46-64. https://doi.org/10.1016/j.dsr.2015.01.007

Lin, P., Wang, F., Chen, Y., & Tang, X. Temporal and spatial variation characteristics of eddies in the South China Sea I: Statistical analyses. Acta Oceanologica Sinica,2007, 29(3), 14-22.

McWilliams, J. Submesoscale currents in the ocean. *Proceedings of the Royal Society A,* 2016, 472, 20160117. http://dx.doi.org/10.1098/rspa.2016.0117

Morison, J., Andersen, R., Larson, N., D'Asaro, E., Boyd, T. The correction for thermal-lag effects in Sea-Bird CTD data. *Journal of Atmospheric and Oceanic Technology*, 1994, 11, 1151–1164, https://doi. org/10.1175/1520-0426(1994)011,1151:TCFTLE.2.0.CO;2.

Morrow, R., Birol, F., Griffin, D., Sudre, J. Divergent pathways of cyclonic and anti-cyclonic ocean eddies. *Geophysical Research Letters*, 2004, *31*(24), L24311. https://doi.org/10.1029/2004gl020974

Nan, F., He, Z., Zhou, H., Wang, D. Three long-lived anticyclonic eddies in the northern South China Sea. *Journal of Geophysical Research: Oceans*, 2011, 116(5), C05002. https://doi.org/10.1029/2010JC006790

Ni, Q., Zhai, X., Wilson, C., Chen, C., Chen, D. Submesoscale eddies in the South China Sea. *Geophysical Research Letters*, 2021, 48, e2020GL091555. https://doi.org/10.1029/2020GL091555

Oey, L. Eddy- and wind-forced shelf circulation. *Journal of Geophysical Research*, 1995, *100*(C5), 8621–8637.https://doi.org/10.1029/95JC00785.

Okkonen, S., Weingartener, T., Danielson, S., Musgrave, D., Schmidt, G. M. Satellite and hydrographic observations of eddy-induced shelf-slope exchange in the northwestern Gulf of Alaska. *Journal of Geophysical Research*, 2003, *108*(C2), 3033. https://doi.org/10.1029/2002JC001342.

Qi, Y., Shang, C., Mao, H., Qiu, C., Shang, X. Spatial structure of turbulent mixing of an anticyclonic mesoscale eddy in the northern South China Sea. *Acta Oceanologica Sinica*, 2020, 39(11), 69-81. https://doi.org/10.1007/s13131-020-1676-z.

Qiao, J., Qiu, C., Wang, D., Huang, Y., Zhang, X., Huang, Y. Multi-stage Development within Anisotropy Insight of an Anticyclone Eddy Northwestern South China Sea in 2021. *Geophysical Research Letter*, 2023, doi:10.1029/2023GL104736

Qiu, C., Mao, H., Yu, J., Xie, Q., Wu, J., Lian, S., Liu, Q. Sea surface cooling in the Northern South China Sea observed using Chinese Sea-wing Underwater Glider Measurements. *Deep Sea Research Part I: Oceanographic Research Papers*, 2015, 105, 111-118.

https://doi.org/10.5194/essd-2024-338
Preprint. Discussion started: 9 September 2024

Qiu, C., Mao, H., Liu, H., Xie, Q., Yu, J., Su, D., Ouyang, J., Lian, S. Deformation of a warm eddy in the northern South China Sea. *Journal of Geophysical Research: Oceans*, 2019, 124, 5551-5564. https://doi.org/10.1029/2019JC015288

Qiu, C., Mao, H., Wang, Y., Su, D., Lian, S. An irregularly shaped warm eddy observed by Chinese underwater gliders. *Journal of Oceanography*, 2019, 75, 139-148.

Qiu, C., Liang, H., Huang, Y., Mao, H., Yu, J., Wang, D., Su, D. Development of double cyclonic mesoscale eddies at around Xisha Islands observed by a 'Sea-Whale 2000' autonomous underwater vehicle. *Applied Ocean Research*, 2020, https://doi.org/10.1016/j.apor.2020.102270.

Qiu, C., Yi, Z., Su, D., Wu, Z., Liu, H., Lin, P., He, Y., Wang, D. Cross-slope heat and salt transport induced by slope intrusion eddy's horizontal asymmetry in the northern South China Sea. *Journal of Geophysical Research: Oceans,* 2022, doi: 10.1029/2022JC018406.

Qiu, C., Yang, Z., Feng, M., Yang, J., Rippeth, T.P., Shang, X., Sun, Z., Jing, C., Wang, D. Observational energy transfers of a spiral cold filament within an anticyclonic eddy. *Progress in Oceanography*, 2024a, https://doi.org/10.1016/j.pocean.2023.103187**.**

Qiu, C., Du, Z., Yu, J., et al. AUG and AUV data used in research "A High Dense Temperature-Salinity Dataset Observed by Automatic Underwater Vehicles toward Mesoscale eddies' Evolutions and Associated Submesoscale Processes in South China Sea" [DS/OL]. V2. Science Data Bank, 2024b[2024-08-03]. https://doi.org/10.57760/sciencedb.11996. DOI: 10.57760/sciencedb.11996.

Rainville, L., Lee, C., Arulananthan, K., Jinadasa, S., Fernando, H., Priyadarshani, W., Wijesekera, H. Water mass exchanges between the Bay of Bengal and Arabian Sea from multiyear sampling with autonomous gliders. *Journal of Physical Oceanography*, 2022, 52, 2377–2396, https://doi.org/10.1175/JPO-D-21-0279.1.

Shang, X., Shu, Y., Wang, D., Yu, J., Mao, H., Liu, D., Qiu, C., Tang, H. Submesoscale motions driven by down-front wind around an anticyclonic eddy with a cold core. *Journal of Geophysical Research: Oceans*, 2023, 128, e2022JC019173. https://doi.org/10.1029/2022JC019173.

Shu, Y., Xiu, P., Xue, H., Yao, J., Yu, J. (2016). Glider-observed anticyclonic eddy in northern South China Sea. *Aquatic Ecosystem Health & Managemen*t, 19(3), 233–241. https://doi.org/10.1080/14634988.2016.1208028

Su, D., Lin, P., Mao, H., Wu, J., Liu, H., Cui, Y., Qiu, C. Features of slope intrusion mesoscale eddies in the northern South China Sea. *Journal of Geophysical Research: Oceans,* 2020, 125, e2019JC015349. https://doi.org/ 10.1029/2019JC015349.

Tang, H., Shu, Y., Wang, D., Xie, Q., Zhang, Z., Li, J., Shang, X., Zhang, O., Liu, D. Submesoscale processes observed by high-frequency float in the western South China Sea. *Deep Sea Research Part I: Oceanographic Research Papers*, 2022, 103896. https://doi.org/10.1016/j.dsr.2022.103896

Thomas, L., Taylor, J., Ferrari, R., Terrence M. Symmetric instability in the Gulf Stream. *Deep Sea Research Part II: Topical Studies in Oceanography*, 2013, 91, 96-110. https://doi.org/10.1016/j.dsr2.2013.02.025

Todd, R.E., Ren, A.S. Warming and lateral shift of the Gulf Stream from in situ observations since 2001. *Nature Climate Change,* 2023, **13**, 1348–1352. https://doi.org/10.1038/s41558-023-01835-w

https://doi.org/10.5194/essd-2024-338
Preprint. Discussion started: 9 September 2024

Wang, G., Su, J., Chu, P. Mesoscale eddies in the South China Sea observed with altimetry. *Geophysical Research Letter*, 2003, 30(21), 2121. doi: 10.1029/2003GL018532.

Wang, G., Chen, D., Su, J. Winter eddy genesis in the eastern South China Sea due to orographic wind jets. *Journal of Physical Oceanography*, 2008, 38(3), 726–732. https://doi.org/10.1175/2007jpo3868.1

Wang, Q., Zeng, L., Li, J., Chen, J., He, Y., Yao, J., Wang, D., Zhou, W. Observed Cross-Shelf Flow Induced by Mesoscale Eddies in the Northern South China Sea. *Journal of Physical Oceanography*, 2018, 48, 1609–1628. https://doi.org/10.1175/JPO-D-17-0180.1

Wang, D., Xu, H., Lin, J., Hu, J. Anticyclonic eddies in the northeastern South China Sea during winter of 2003/2004. *Journal of Oceanography*, 2008, 64(6), 925-935

Wang, Z., Chen, Q. Warm core eddies in the northern South China Sea (I): Preliminary observations of warm eddies in the South China Sea. J*ournal of Oceanography of Taiwan Strait*,1987, 18, 92-103.

Xu, J., Su, J. Hydrographic analysis of Kuroshio intrusion into the South China Sea II: Observations during August-September 1994. *Tropical Oceanography*,1997, 2, 1-23.

Yang, H., Liu, Q. The seasonal features of temperature distributions in the upper layer of the South China Sea. *Oceanologia et Limnologia Sinica*, 1998,29(5), 501-507.

Xiu, P., Chai, F., Shi, L., Xue, H., Chao, Y. A census of eddy activities in the South China Sea during 1993-2007. *Journal of Geophysical Research: Oceans*, 2010,115, C03012. doi: 10.1029/2009JC005657.

Yang, Q., Nikurashin, M., Sasaki, H., Sun, H., Tian, J. Dissipation of mesoscale eddies and its contribution to mixing in the northern South China Sea. *Scientific Reports*, 2019, 9. https://doi.org/10.1038/s41598-018-36610-x

Yi, Z., Wang, D., Qiu, C., Mao, H., Yu, J., Lian, S. Variations in dissolved oxygen induced by a tropical storm within an anticyclone in the Northern South China Sea. *Journal of Ocean University of China*, 2022, 21(5), 1084-1098. https://doi.org/10.1007/s11802-022-4992-4.

Zhang, Z., Qiu, B. Evolution of submesoscale ageostrophic motions through the life cycle of oceanic mesoscale eddies. *Geophysical Research Letters,* 2018, 45(21), 11847-11855. https://doi.org/10.1029/2018GL080399

Zhang, Z., Tian, J., Qiu, B., Zhao, W., Chang, P., Wu, D. Observed 3D Structure, Generation, and Dissipation of Oceanic Mesoscale Eddies in the South China Sea. *Scientific Reports,* 2016, 6(1), 24349. https://doi.org/10.1038/srep24349

Zhang, Z., Zhao, W., Qiu, B., Tian, J. Anticyclonic eddy sheddings from Kuroshio loop and the accompanying cyclonic eddy in the Northeastern South China Sea. *Journal of Physical Oceanography*, 2017, 47(6), 1243-1259. https://doi.org/10.1175/JPO-D-16-0185.1